

Total internal reflection microscopy with a multilayered interface: a light scattering model based on a discrete sources method

Elena Eremina¹, Natalia Grishina², Yuri Eremin², Laurent Helden³
and Thomas Wriedt⁴

¹ University of Bremen, Badgasteiner strasse 3, 28359 Bremen, Germany

² Moscow Lomonosov State University, Vorobyov's Hills, 119992 Moscow, Russia

³ 2. Physikalisches Institut, University of Stuttgart, Pfaffenwaldring 57, 70550 Stuttgart, Germany

⁴ Institut für Werkstofftechnik, Badgasteiner strasse 3, 28359 Bremen, Germany

E-mail: eremina@iwt.uni-bremen.de

Received 11 July 2006, accepted for publication 28 September 2006

Published 18 October 2006

Online at stacks.iop.org/JOptA/8/999

Abstract

The discrete sources method has been extended to analyse *P* or *S* polarized evanescent wave scattering by a dielectric particle located on a layered interface. This was done to develop a light scattering simulation model for total internal reflection microscopy. The influence of metallic layers on the prism surface is investigated. Numerical results for the objective response versus particle height and the scattering cross-section are presented.

Keywords: total internal reflection microscopy, evanescent waves scattering, layered interface, discrete sources method

(Some figures in this article are in colour only in the electronic version)

1. Introduction

Since its invention in the mid-1980s [1] total internal reflection microscopy (TIRM) has proven to be an extremely sensitive technique for measuring weak interaction forces between colloidal particles and plane surfaces with a resolution down to a few femtonewtons [2]. Compared to other methods for measuring colloidal interactions like using the surface force apparatus [3] and atomic force microscopy [4], TIRM is the more sensitive technique because it utilizes the Brownian fluctuations of a free colloidal particle to deduce the interaction potential. Reviews of the state of the TIRM technique can be found in [5–7].

In TIRM-based experiments typically there is water containing colloidal particles situated near a glass prism. A laser beam propagating in the prism hits the prism–water interface at an angle slightly above the angle of total internal reflection. As a result an evanescent field appears close to the surface. Particles dispersed in the water start to scatter evanescent light and a detector registers its intensity. The scattering intensity contains information about the particle and

its distance from the surface. For analysis of the measured signals the TIRM method requires precise knowledge of the particle–wall distance dependence of the scattering intensity. For this purpose modern modelling methods can be used. The discrete sources method (DSM) [8, 9] has already been applied to model TIRM experiments. In [10] measurement results have been compared to the DSM model for a prism. To enlarge the spectrum of substrates suitable for TIRM, gold (Au) coated substrates are of interest. They can easily be functionalized with self-assembled monolayers via thiol bonds [11]. The functionalization will enable measurements with biologically functionalized surfaces. Films in particular increase the scattering cross-section [12]. For technical reasons an additional layer of titanium (Ti) or chrome (Cr) is required in between glass and gold to modify the wetting properties of the Au coating from non-wetting to wetting. In this paper we present a modification of the DSM, which allows taking into account multilayered structure deposited on the prism surface.

In the following sections we will discuss the theoretical foundations of the DSM. In the last section of the paper we

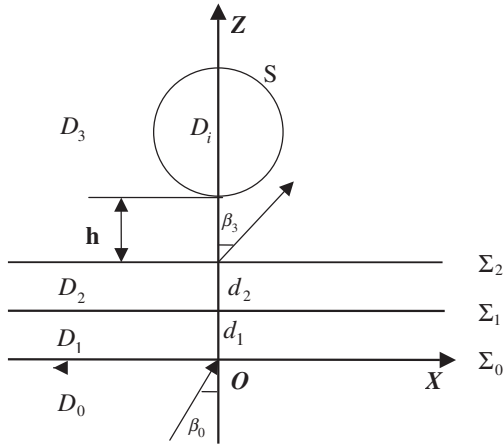


Figure 1. Model geometry: a particle deposited on a layered glass surface.

present numerical results; a short discussion is given in the last section as well.

2. Discrete sources method

In this section the DSM model for evanescent wave scattering analysis is considered. We start with the mathematical statement of the polarized light scattering problem. Consider a spherical penetrable particle with interior domain D_i and smooth boundary S that is deposited above the plane surface Σ_2 ($z = d_2$) of a final layer (figure 1).

We denote the prism domain by D_0 and the ambient space exterior to the particle by D_3 . Let us introduce a Cartesian coordinate system $Oxyz$ by choosing its origin O at the intersection point of the axis of symmetry of the particle and the plane Σ_0 ($z = 0$). The z -axis coincides with the axis of symmetry of the particle and is directed into domain D_3 . A titanium (Ti) film occupying domain D_1 with upper boundary Σ_1 ($z = d_1$) is located on planar surface Σ_0 of a glass prism. A gold (Au) film occupying domain D_2 with upper boundary Σ_2 is located on the Ti film. We assume that the exciting field $\{\mathbf{E}_0, \mathbf{H}_0\}$ is a linear polarized plane wave propagating inside the glass prism at angle β_0 with respect to the z -axis. According to the Snell's law the wave $\{\mathbf{E}_3^i, \mathbf{H}_3^i\}$ refracted into D_3 propagates at angle β_3 to the z -axis. Then the mathematical statement of the scattering problem can be formulated in the following form:

$$\begin{aligned} \nabla \times \mathbf{H}_l &= jk\varepsilon_l \mathbf{E}_l, & \nabla \times \mathbf{E}_l &= -jk\mu_l \mathbf{H}_l, \\ & \text{in } D_l, \quad l = \overline{0, 3}, i, \\ \mathbf{n} \times (\mathbf{E}_i - \mathbf{E}_3) &= 0 & \mathbf{n} \times (\mathbf{H}_i - \mathbf{H}_3) &= 0 & \text{at } S \\ \mathbf{e}_z \times (\mathbf{E}_{l+1} - \mathbf{E}_l) &= 0 & \mathbf{e}_z \times (\mathbf{H}_{l+1} - \mathbf{H}_l) &= 0 \\ & \text{at } \Sigma_l \quad \text{where } l = \overline{0, 2}, i \end{aligned} \quad (1)$$

and radiation (attenuation) conditions at infinity in D_3 .

Here, \mathbf{n} is the outward unit vector normal to S , $k = \omega/c$ and $\{\mathbf{E}_l, \mathbf{H}_l\}$ stands for the total field in the corresponding domain D_l , \mathbf{e}_z is the unit vector along the z -axis. Note that the total field in D_3 is a superposition of the refracted exciting

field and the scattered one, that is $\mathbf{E}_3 = \mathbf{E}_3^s + \mathbf{E}_3^i$, $\mathbf{H}_3 = \mathbf{H}_3^s + \mathbf{H}_3^i$. If $\text{Im } \varepsilon_\zeta, \mu_\zeta \leq 0$ (the time dependence for the fields is chosen as $\exp[j\omega t]$) and the particle surface is smooth enough, $S \subset C^{(2,\alpha)}$, then the above boundary value problem is uniquely solvable.

The solution of the boundary value problem is constructed following the DSM scheme [9]. First the diffraction problem of the plane wave on the layered interface is solved. The resulting field $\{\mathbf{E}_l^i, \mathbf{H}_l^i\}$ satisfies all the boundary conditions at $\Sigma_{0,1,2}$. Then we construct an approximate solution to the scattering problem (1) via the DSM by representing the electromagnetic fields as a finite linear combination of the fields of dipoles and multipoles which satisfy analytically the transmission conditions enforced at the plane interfaces $\Sigma_{0,1,2}$ [13]. The approximate solution satisfies the Maxwell equations in the domains D_l , $l = \overline{0, 3}$, infinity conditions and the transmission conditions at the interfaces $\Sigma_{0,1,2}$. Thus, the scattering problem is reduced to the problem of approximating the exciting field on the particle surface S . The amplitudes of discrete sources are determined from the boundary conditions at the particle surface, which can be rewritten as

$$\mathbf{n} \times (\mathbf{E}_i - \mathbf{E}_3^s) = \mathbf{n} \times \mathbf{E}_3^i, \quad \mathbf{n} \times (\mathbf{H}_i - \mathbf{H}_3^s) = \mathbf{n} \times \mathbf{H}_3^i \quad \text{at } S. \quad (2)$$

To construct the fields of dipoles and multipoles that analytically satisfy the transmission conditions at the plane interfaces $\Sigma_{0,1,2}$ we apply the Green's tensor for a stratified interface [13].

An approximate solution of the scattering problem is constructed fulfilling the transmission conditions on plane interfaces $\Sigma_{0,1,2}$, taking into account the rotational symmetry of the scattering problem geometry (particle plus layered interface) and polarization of the exciting field [9].

First, let us consider a P polarized exciting plane wave. In this case, the refracted plane wave in D_3 adopts the following form:

$$\mathbf{E}_3^i(\mathbf{r}) = T_3^P (-\mathbf{e}_x \cos \beta_3 + \mathbf{e}_z \sin \beta_3) \exp\{-jk_3(x \sin \beta_3 + z \cos \beta_3)\}, \quad (3)$$

$$\mathbf{H}_3^i(\mathbf{r}) = T_{3L}^P n_3 \mathbf{e}_y \exp\{-jk_3(x \sin \beta_3 + z \cos \beta_3)\},$$

where $(\mathbf{e}_x, \mathbf{e}_y, \mathbf{e}_z)$ are unit vectors of the Cartesian coordinate system, $n_3 = \sqrt{\varepsilon_3 \mu_3}$ is the refractive index of the ambient space and T_3^P is the transmission coefficient for P polarization corresponding to the multilayered interface considering Snell's law: $n_0 \sin \beta_0 = n_3 \sin \beta_3$. If $\beta_0 > \beta_c = \arcsin(n_3/n_0)$ the exciting wave is totally reflected from plane Σ_2 and only an evanescent wave expanding along surface Σ_2 and damped along the \mathbf{e}_z direction is present in D_3 . It follows from Snell's law that in this case $\cos \beta_3$ becomes purely imaginary. We must choose its value as $\cos \beta_3 = -j\sqrt{\sin^2 \beta_3 - 1}$, since otherwise the amplitude of the refracted wave would tend to infinity with increasing distance from the interface Σ_2 . So the plane wave looks like $\exp\{-jk_3 x \sin \beta_3\} \exp\{-k_3 z \sqrt{\sin^2 \beta_3 - 1}\}$.

As mentioned above, the approximate solution of the scattering problem is constructed by taking into account not only the rotational symmetry of the scattering problem geometry, but also the polarization of the external excitation [9].

For P polarized excitation we will use the Fourier series for the plane wave with respect to the angle φ :

$$\begin{aligned} & \exp\{-jk_e \rho \sin \beta_3 \cos \varphi\} \\ &= \sum_{m=0}^{\infty} (2 - \delta_{0m}) (-j)^m J_m(k_e \rho \sin \beta_3) \cos m\varphi. \end{aligned}$$

For the Fourier harmonics of the τ , φ field components we get

$$\mathbf{E}_3^i \cdot \boldsymbol{\tau} = e_{m+1}^{P,\tau}(\eta) \cos(m+1)\varphi,$$

$$\mathbf{E}_3^i \cdot \mathbf{e}_\varphi = e_{m+1}^{P,\varphi}(\eta) \sin(m+1)\varphi,$$

$$\mathbf{H}_3^i \cdot \boldsymbol{\tau} = h_{m+1}^{P,\tau}(\eta) \sin(m+1)\varphi,$$

$$\mathbf{H}_3^i \cdot \mathbf{e}_\varphi = h_{m+1}^{P,\varphi}(\eta) \cos(m+1)\varphi,$$

where $\boldsymbol{\tau}$ is a vector tangential to the generatrix \mathfrak{S} and \mathbf{e}_φ is a unit vector of the cylindrical coordinate system.

According to this we use for a P polarized exciting plane wave (3) the following electric and magnetic vector potentials corresponding to the multipoles:

$$\mathbf{A}_{mn}^{e,0}(\mathbf{r}) = \{g_m^e(\eta, z_n) \cos(m+1)\varphi; -g_m^e(\eta, z_n) \sin(m+1)\varphi; -f_{m+1}(\eta, z_n) \cos(m+1)\varphi\},$$

$$\mathbf{A}_{mn}^{h,0}(\mathbf{r}) = \{g_m^h(\eta, z_n) \sin(m+1)\varphi; g_m^h(\eta, z_n) \cos(m+1)\varphi; -f_{m+1}(\eta, z_n) \sin(m+1)\varphi\},$$

$$\mathbf{A}_{0n}^{e,h,0}(\mathbf{r}) = \{0; 0; g_0^{e,h}(\eta, z_n)\};$$

(4)

where $g_m^{e,h}$, f_m are the Fourier harmonics relating to the Green tensor Fourier components, which adopt the form of Weyl-Sommerfeld integrals:

$$\begin{aligned} g_m^{e,h}(\eta, z_n) &= \int_0^\infty J_m(\lambda \rho) v_{11}^{e,h}(z, z_n, \lambda) \lambda^{1+m} d\lambda, \\ f_m(\eta, z_n) &= \int_0^\infty J_m(\lambda \rho) v_{31}(z, z_n, \lambda) \lambda^{1+m} d\lambda. \end{aligned} \quad (5)$$

Here J_m is the cylindrical Bessel function, (ρ, φ, z) are the cylindrical coordinates, point $\eta = (\rho, z)$ belongs to the semi-plane $\varphi = 0$, $R_{\eta z_n}^2 = \rho^2 + (z - z_n)^2$, while $\{z_n\}_{n=1}^\infty$ is a dense set of discrete source points distributed over a segment $\Gamma_z^0 \in D_i$ of the axis of symmetry and $v_{11}^{e,h}(z, z_n, \lambda)$, $v_{31}(z, z_n, \lambda)$ are the corresponding spectral functions. The spectral functions provide the continuity of the field tangential components at the interfaces $\Sigma_{0,1,2}$ and can be represented as

$$v_{11}^{e,h} = \begin{cases} \frac{\exp\{-\eta_3 |z - z_n|\}}{\eta_3} + A_3^{e,h+}(\lambda, z_n) \exp\{-\eta_3 |z - d_2|\}, & z \geq d_2, z_n > 0 \\ A_l^{e,h-}(\lambda, z_n) \exp\{-\eta_l |z - d_{l+1}|\} \\ \quad + A_l^{e,h+}(\lambda, z_n) \exp\{-\eta_l |z - d_l|\}, & d_{l+1} \geq z \geq d_l; \\ A_0^{e,h-}(\lambda, z_n) \exp\{\eta_0 z\}, & z \leq 0 \end{cases}$$

$$v_{31}^{e,h} = \begin{cases} B_3^{e,h+}(\lambda, z_n) \exp\{-\eta_3 |z - d_2|\}, & z \geq d_2, z_n > 0 \\ B_l^{e,h-}(\lambda, z_n) \exp\{-\eta_l |z - d_{l+1}|\} \\ \quad + B_l^{e,h+}(\lambda, z_n) \exp\{-\eta_l |z - d_l|\}, & d_{l+1} \geq z \geq d_l; \\ B_0^{e,h-}(\lambda, z_n) \exp\{\eta_0 z\}, & z \leq 0 \end{cases}$$

where $\eta_\zeta^2 = \lambda^2 - k_\zeta^2$. The spectral coefficients A and B can be determined from the one-dimensional transmission conditions at $z = d_l$, $l = 0, 2$, which adopt the form [9]

$$[v_{11}^e] = \left[\frac{1}{\mu} \frac{\partial v_{11}^e}{\partial z} \right] = 0, \quad [v_{11}^e] = \left[\frac{1}{\varepsilon} \frac{\partial v_{11}^e}{\partial z} \right] = 0,$$

$$\left[\frac{1}{\mu} v_{31}^e \right] = 0, \quad \left[\frac{1}{\varepsilon \mu} \frac{\partial v_{31}^e}{\partial z} \right] = \left[\frac{1}{\varepsilon \mu} \right] v_{11}^e,$$

$$\left[\frac{1}{\varepsilon} v_{31}^h \right] = 0, \quad \left[\frac{1}{\varepsilon \mu} \frac{\partial v_{31}^h}{\partial z} \right] = \left[\frac{1}{\varepsilon \mu} \right] v_{11}^h.$$

where $[]$ is a jump of values. In particular, the equality $v_{31}^e = v_{31}^h$ holds at $z \geq d_2$.

For the total field inside particle D_i we determine the following vector potentials [9]:

$$\mathbf{A}_{mn}^{e,i}(\mathbf{r}) = \{J_m^i(\eta, z_n) \cos(m+1)\varphi;$$

$$-J_m^i(\eta, z_n) \sin(m+1)\varphi; 0\},$$

$$\mathbf{A}_{mn}^{h,i}(\mathbf{r}) = \{J_m^i(\eta, z_n) \sin(m+1)\varphi;$$

(6)

$$J_m^i(\eta, z_n) \cos(m+1)\varphi; 0\},$$

$$\mathbf{A}_{0n}^{e,h,i}(\mathbf{r}) = \{0; 0; J_0^i(\eta, z_n)\};$$

where $J_m^i(\eta, z_n) = j_m(k_i R_{\eta z_n}) (\rho / R_{\eta z_n})^m$, and j_m are the spherical Bessel functions. We now introduce the following notation:

$$\overset{\leftrightarrow}{\mathbf{R}}_1^\zeta = \begin{pmatrix} j/k\varepsilon_\zeta \mu_\zeta & \nabla \times \nabla \times \\ -1/\mu_\zeta & \nabla \times \end{pmatrix},$$

$$\overset{\leftrightarrow}{\mathbf{R}}_2^\zeta = \begin{pmatrix} 1/\varepsilon_\zeta \eta & \nabla \times \\ j/k\varepsilon_\zeta \mu_\zeta & \nabla \times \nabla \times \end{pmatrix}.$$

By this, we can represent the approximate solution of the scattering problem for the P polarized excitation as [13]

$$\begin{aligned} \begin{pmatrix} \mathbf{E}_N^\zeta \\ \mathbf{H}_N^\zeta \end{pmatrix} &= \sum_{m=0}^M \sum_{n=1}^{N_m^\zeta} \left\{ p_{mn}^\zeta \overset{\leftrightarrow}{\mathbf{R}}_1^\zeta \mathbf{A}_{mn}^{e,\zeta} + q_{mn}^\zeta \overset{\leftrightarrow}{\mathbf{R}}_2^\zeta \mathbf{A}_{mn}^{h,\zeta} \right\} \\ &+ \sum_{n=1}^{N_m^\zeta} r_n^\zeta \overset{\leftrightarrow}{\mathbf{R}}_1^\zeta \mathbf{A}_n^{e,\zeta}; \quad \zeta = 3, i. \end{aligned} \quad (7)$$

The last term in (7) is associated with vertical electric dipoles. Here, N is a complex index incorporating M and N_m^ζ . Let us emphasize that in the frame of the DSM, the scattered field $\{\mathbf{E}_N^\zeta, \mathbf{H}_N^\zeta\}$ in domains $D_{0,1,2,3}$ can be represented in terms of the unitary set of amplitudes $\{p_{mn}^3, q_{mn}^3, r_n^3\}$ after the transmission conditions at the interfaces $\Sigma_{0,1,2}$ are satisfied using Green's tensor components (5) [13].

Let us consider next S polarization of the exciting plane wave

$$\begin{aligned} \mathbf{E}_3^i(\mathbf{r}) &= T_3^S \mathbf{e}_y \exp\{-jk_3(x \sin \beta_3 + z \cos \beta_3)\}, \\ \mathbf{H}_3^i(\mathbf{r}) &= T_3^S n_3 (-\mathbf{e}_x \cos \beta_3 + \mathbf{e}_z \sin \beta_3) \\ &\times \exp\{-jk_3(x \sin \beta_3 + z \cos \beta_3)\}, \end{aligned} \quad (8)$$

where the T_3^S Fresnel coefficients associated with interfaces $\Sigma_{0,1,2}$.

The Fourier components are taking the form

$$\begin{aligned} \mathbf{E}^0 \cdot \boldsymbol{\tau} &= e_{m+1}^{S,\tau}(\eta) \sin(m+1)\varphi, \\ \mathbf{E}^0 \cdot \mathbf{e}_\varphi &= e_{m+1}^{S,\varphi}(\eta) \cos(m+1)\varphi \\ \mathbf{H}^0 \cdot \boldsymbol{\tau} &= h_{m+1}^{SE,\tau}(\eta) \cos(m+1)\varphi, \\ \mathbf{H}^0 \cdot \mathbf{e}_\varphi &= h_{m+1}^{S,\varphi}(\eta) \sin(m+1)\varphi. \end{aligned}$$

To take into account the polarization of the external excitation in the S case (8) we use the following electric and magnetic potentials:

$$\begin{aligned} \mathbf{A}_{mn}^{e,0}(\mathbf{r}) &= \{g_m^e(\eta, z_n) \sin(m+1)\varphi; g_m^e(\eta, z_n) \cos(m+1)\varphi; \\ &-f_{m+1}(\eta, z_n) \sin(m+1)\varphi\}, \\ \mathbf{A}_{mn}^{h,0}(\mathbf{r}) &= \{g_m^h(\eta, z_n) \cos(m+1)\varphi; -g_m^h(\eta, z_n) \sin(m+1)\varphi; \\ &-f_{m+1}(\eta, z_n) \cos(m+1)\varphi\}, \\ \mathbf{A}_{0n}^{e,h,0}(\mathbf{r}) &= \{0; 0; g_0^{h,e}(\eta, z_n)\}. \end{aligned} \quad (9)$$

So, for S polarization the approximate solution adopts the following form:

$$\begin{aligned} \begin{pmatrix} \mathbf{E}_N^\zeta \\ \mathbf{H}_N^\zeta \end{pmatrix} &= \sum_{m=0}^M \sum_{n=1}^{N_m^\zeta} \left\{ p_{mn}^\zeta \overset{\leftarrow}{\mathbf{R}}_1^\zeta \mathbf{A}_{mn}^{e,\zeta} + q_{mn}^\zeta \overset{\leftarrow}{\mathbf{R}}_2^\zeta \mathbf{A}_{mn}^{h,\zeta} \right\} \\ &+ \sum_{n=1}^{N_m^\zeta} r_n^\zeta \overset{\leftarrow}{\mathbf{R}}_2^\zeta \mathbf{A}_n^{h,\zeta}; \quad \zeta = 3, i. \end{aligned} \quad (10)$$

The last term in (10) is associated with vertical magnetic dipoles [14]. The difference between (7) and (10) is caused by the fact that for S polarization vector \mathbf{H}_3^i belongs to the incident plane.

The completeness of the system of lowest order distributed multipoles used in (7), (10) guarantees the convergence of the approximate solution to the exact one in any closed subset of D_3 [9].

As mentioned above, representations (7), (10) satisfy all the conditions of the scattering problem (1) except the transmission conditions at the particle surface (2). These conditions are employed to determine the amplitudes of discrete sources $\{p_{mn}^{3,i}, q_{mn}^{3,i}, r_n^{3,i}\}$. Since the scattering problem geometry is axially symmetric with respect to the z -axis and the discrete sources are distributed along the axis of symmetry, fulfilling the transmission conditions (2) at surface S can be reduced to the sequential solution of the transmission problems for the Fourier harmonics of the fields. So, instead of matching the fields on the scattering surface (see (2)), we can match their Fourier harmonics, thus reducing the approximation problem on the surface to a set of problems enforced at the particle surface generatrix \mathfrak{S} . The unknown

vector of discrete source's amplitudes $\{p_{mn}^{3,i}, q_{mn}^{3,i}, r_n^{3,i}\}$ can be determined as a pseudosolution of an overdetermined system of linear equations

$$\mathbf{B}_m \mathbf{p}_m = \mathbf{q}_m, \quad m = 0, \dots, M.$$

Here \mathbf{B}_m is a rectangular matrix $\mathbf{B}_m = [B_{ji}^m]$, $j = 1, \dots, 4L$, $i = 1, \dots, 2(N_i^m + N_3^m)$. The reasonable ratio of matching points and number of DS was established as $2 < L/(N_i^m + N_3^m) < 4$. The vector of unknown amplitudes \mathbf{p}_m has the length $2(N_i^m + N_3^m)$ and the vector in the right-hand side can be represented as $4L$ vector in the following form:

$$\mathbf{q}_m = \left(e_{m+1,l}^{0\tau}, e_{m+1,l}^{0\varphi}, h_{m+1,l}^{0\tau}, h_{m+1,l}^{0\varphi} \right)^T,$$

where

$$e_{m+1,l}^{0\tau} = e_{m+1,l}^{0\tau}(\eta_l), \quad h_{m+1,l}^{0\tau} = h_{m+1,l}^{0\tau}(\eta_l).$$

The components of the vector for the P polarized excitation can be written as

$$\begin{aligned} e_{m+1,l}^{0\tau}(\eta) &= \alpha \cos \beta_3 (-j)^m T_3^P [J_m(k_3 \rho \sin \beta_3) \\ &- J_{m+2}(k_3 \rho \sin \beta_3) + 2j\gamma \sin \beta_3 J_{m+1}(k_3 \rho \sin \beta_3)] \\ &\times n_3 \exp\{-jk_3 z \cos \beta_3\}, \\ e_{m+1,l}^{0\varphi}(\eta) &= -\cos \beta_3 (-j)^m T_3^P [J_m(k_3 \rho \sin \beta_3) \\ &+ J_{m+2}(k_3 \rho \sin \beta_3)] n_3 \exp\{-jk_3 z \cos \beta_3\}, \\ h_{m+1,l}^{0\tau}(\eta) &= -\alpha (-j)^m T_3^P [J_m(k_3 \rho \sin \beta_3) \\ &+ J_{m+2}(k_3 \rho \sin \beta_3)] n_3 \exp\{-jk_3 z \cos \beta_3\}, \\ h_{m+1,l}^{0\varphi}(\eta) &= (-j)^m T_3^P [-J_m(k_3 \rho \sin \beta_3) \\ &+ J_{m+2}(k_3 \rho \sin \beta_3)] n_3 \exp\{-jk_3 z \cos \beta_3\} \end{aligned}$$

where T_3^P is calculated using the following recursion [15]:

$$\begin{aligned} r_i &= \frac{n_{i-1} \cos \beta_i - n_i \cos \beta_{i-1}}{n_{i-1} \cos \beta_i + n_i \cos \beta_{i-1}}, \\ t_i &= \frac{2n_{i-1} \cos \beta_{i-1}}{n_{i-1} \cos \beta_i + n_i \cos \beta_{i-1}}, \end{aligned}$$

$$R_L = 0,$$

$$R_{L-1} = r_L, \quad R_i = \frac{r_{i+1} + R_{i+1} \exp\{-2\delta_{i+1}\}}{1 + r_{i+1} R_{i+1} \exp\{-2\delta_{i+1}\}},$$

$$i = \overline{L-2, 0}.$$

$$T_1 = t_1, \quad T_{i+1} = \frac{T_i t_{i+1} \exp\{-\delta_i\}}{1 + r_i R_i \exp\{-2\delta_i\}},$$

$$i = \overline{1, L-1}.$$

$$T_3^P = T_L.$$

Here r_i and t_i are the coefficients of reflection and refraction on the boundary Σ_i respectively and R_i and T_i are the coefficients of reflection and refraction in media D_{i+1} , taking into account the layered interface $\delta_i = d_{i+1} - d_i$.

In the case of S polarized excitation the components are presented in the form

$$\begin{aligned} e_{m+1,l}^{0\tau}(\eta) &= \alpha (-j)^m T_3^S [J_m(k_3 \rho \sin \beta_3) \\ &+ J_{m+2}(k_3 \rho \sin \beta_3)] n_3 \exp\{-jk_3 z \cos \beta_3\}, \\ e_{m+1,l}^{0\varphi}(\eta) &= (-j)^m T_3^S [J_m(k_3 \rho \sin \beta_3) \\ &- J_{m+2}(k_3 \rho \sin \beta_3)] n_3 \exp\{-jk_3 z \cos \beta_3\}, \\ h_{m+1,l}^{0\tau}(\eta) &= \alpha \cos \beta_0 (-j)^m T_3^S [J_m(k_3 \rho \sin \beta_3) \end{aligned}$$

$$\begin{aligned}
 & - J_{m+2}(k_3 \rho \sin \beta_3) + 2j\gamma \sin \beta_3 J_{m+1}(k_3 \rho \sin \beta_3) \\
 & \times n_3 \exp\{-jk_3 z \cos \beta_3\}, \\
 h_{m+1,l}^{0\varphi}(\eta) = & -\cos \beta_3 (-j)^m T_3^S [J_m(k_3 \rho \sin \beta_3) \\
 & + J_{m+2}(k_3 \rho \sin \beta_3)] n_3 \exp\{jk_3 z \cos \beta_3\},
 \end{aligned}$$

where

$$\begin{aligned}
 r_i &= \frac{n_{i-1} \cos \theta_{i-1} - n_i \cos \theta_i}{n_{i-1} \cos \theta_{i-1} + n_i \cos \theta_i}, \\
 t_i &= \frac{2n_{i-1} \cos \theta_{i-1}}{n_{i-1} \cos \theta_{i-1} + n_i \cos \theta_i}.
 \end{aligned}$$

Here $(\alpha, 0, \gamma)$ is a vector, tangential to the generatrix at the η -point, (ρ, z) are the coordinates of the matching point. Because the Fourier harmonics do not depend on the φ -angle, the linear system corresponding to vertical electric or magnetic dipoles for both polarizations can be written as

$$\mathbf{B}_{-1} \mathbf{p}_{-1} = \mathbf{q}_{-1}$$

where \mathbf{B}_{-1} has the dimension of $2L \times (N_i^m + N_3^m)$, the right-hand side vector has the length $2L$ and the unknown vector of amplitudes has length $(N_i^m + N_3^m)$.

Then for P polarization we have

$$\begin{aligned}
 e_0^{0\varphi}(\eta) &= -jT_3^P [\alpha \cos \theta_3 J_1(k_3 \rho \sin \theta_3) \\
 & + \beta \sin \theta_3 J_0(k_3 \rho \sin \theta_3)] \exp\{-jk_3 z \cos \theta_3\}, \\
 h_0^{0r}(\eta) &= jT_3^P J_1(k_3 \rho \sin \theta_3) \exp\{-jk_3 z \cos \theta_3\} n_3.
 \end{aligned}$$

And for S polarization

$$\begin{aligned}
 e_0^{0r}(\eta) &= jT_3^S J_1(k_3 \rho \sin \theta_3) \exp\{-jk_3 z \cos \theta_3\}, \\
 h_0^{0\varphi}(\eta) &= -jT_3^S [\alpha \cos \theta_3 J_1(k_3 \rho \sin \theta_3) \\
 & + \beta \sin \theta_3 J_0(k_3 \rho \sin \theta_3)] \exp\{-jk_3 z \cos \theta_3\} n_3.
 \end{aligned}$$

As DSM is a direct method it allows one to solve the scattering problem for the entire set of incident angles β_0 and both polarizations (P and S) at once. Besides, the numerical scheme provides an opportunity to control the convergence of the approximate solution by posterior error estimation [9].

After the amplitudes of the discrete sources are determined, one can compute the far field pattern $\mathbf{F}(\theta, \phi)$ of the scattered field, which is determined at the upper part of the unit semi-sphere $\Omega = \{0^\circ \leq \theta < 90^\circ, 0^\circ \leq \varphi \leq 360^\circ\}$ and is given by

$$\mathbf{E}_3^s(\mathbf{r})/\mathbf{E}^0(0) = \frac{\exp\{jk_0 r\}}{r} \mathbf{F}(\theta, \varphi) + O(r^{-2}) \quad z > 0, \\
 r \rightarrow \infty.$$

$$\text{Here } \mathbf{F}^{P,S}(\theta, \varphi) = F_\theta^{P,S} \mathbf{e}_\theta + F_\varphi^{P,S} \mathbf{e}_\varphi.$$

By asymptotical estimation of the Weyl–Sommerfeld integrals involved in (5) the representation of the elements of the far field pattern takes the form of a finite linear combination

of elementary functions [9]:

$$\begin{aligned}
 F_\theta^P(\theta, \varphi) &= jk_3 \sum_{m=0}^M \cos[(m+1)\varphi] (jk_3 \sin \theta)^m \\
 & \times \sum_{n=1}^{N_0^m} \{p_{nm}^0 \cos \theta [\gamma'_n + (v_n^e - v_n \sin^2 \theta) \gamma_n] \\
 & + q_{nm}^0 (\gamma' + v_n^h \gamma_n)\} - jk_3 \sin \theta \sum_{n=1}^{N_0^0} r_n^0 (\gamma' + v_n^h \gamma_n), \quad (11)
 \end{aligned}$$

$$\begin{aligned}
 F_\varphi^P(\theta, \varphi) &= -jk_3 \sum_{m=0}^M \sin[(m+1)\varphi] (j \sin \theta)^m \\
 & \times \sum_{n=1}^{N_0^m} \{p_{nm}^0 (\gamma' + v_n^h \gamma_n) \\
 & + q_{nm}^0 \cos \theta [\gamma'_n + (v_n^e - v \sin^2 \theta) \gamma_n]\},
 \end{aligned}$$

and for S polarized excitation following representation (10) one gets

$$\begin{aligned}
 F_\theta^S(\theta, \varphi) &= jk_3 \sum_{m=0}^M \sin[(m+1)\varphi] (j \sin \theta)^m \\
 & \times \sum_{n=1}^{N_0^m} \{p_{nm}^0 \cos \theta [\gamma'_n + (v_n^e - v \sin^2 \theta) \gamma_n] \\
 & - q_{nm}^0 (\gamma' + v_n^h \gamma_n)\}, \\
 F_\varphi^S(\theta, \varphi) &= jk_3 \sum_{m=0}^M \cos[(m+1)\varphi] (j \sin \theta)^m \\
 & \times \sum_{n=1}^{N_0^m} \{p_{nm}^0 \cos \theta [\gamma'_n + (v_n^e - v \sin^2 \theta) \gamma_n] \\
 & - q_{nm}^0 (\gamma' + v_n^h \gamma_n)\} + jk_3 \sin \theta \sum_{n=1}^{N_0^0} r_n^0 (\gamma' + v_n^e \gamma_n), \quad (12)
 \end{aligned}$$

where the corresponding spectral functions adopt the form

$$\begin{aligned}
 v_n^e(\theta, z_n) &= jk_3 \cos \theta \exp\{jk_3 d_2 \cos \theta\} A_{11}^{e,h}(k_3 \sin \theta, z_n), \\
 v_n^h(\theta, z_n) &= jk_3 \cos \theta \exp\{jk_3 d_2 \cos \theta\} A_{31}^{e,h}(k_3 \sin \theta, z_n), \\
 \gamma_n &= \exp\{-jk_3 z_n \cos \theta\}, \quad \gamma'_n = \exp\{jk_3 z_n \cos \theta\}.
 \end{aligned}$$

Hence, after the unknown amplitudes of discrete sources are determined, far field patterns for P/S polarization (11) and (12) are represented as finite linear combinations of elementary functions. This circumstance ensures fast and effective computer analysis of the scattering characteristics in the wave zone.

3. Results and discussion

In this section we present computer simulation results for the conversion of evanescent waves into scattered ones by a particle deposited on a metal-filmed glass prism. We consider

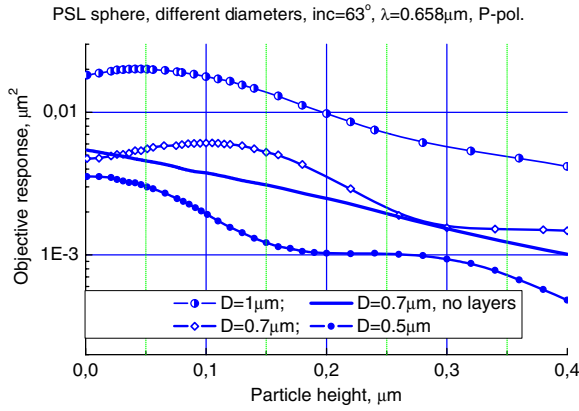


Figure 2. Objective response (14) versus particle height (h) for different particle diameters in the presence of layers and without; P polarization.

the differential scattering cross-section (DSC), which is given by

$$\text{DSC}^{P,S}(\beta_0, \theta, \varphi) = \left| F_{\theta}^{P,S}(\beta_0, \theta, \varphi) \right|^2 + \left| F_{\varphi}^{P,S}(\beta_0, \theta, \varphi) \right|^2. \quad (13)$$

Here $F_{\theta, \varphi}^{P,S}(\theta, \varphi)$ are the components of the far field pattern (11), (12) corresponding to the P/S polarized excitation measured in μm^2 . In this paper we will also examine the objective response function, which is plotted as a function of height. It represents the integrated intensity scattered into the prescribed solid angle

$$\sigma_S(\beta_0) = \int_{\Omega} \text{DSC}^{P,S}(\beta_0, \theta, \varphi) d\omega, \quad (14)$$

where $\Omega = \{0^\circ \leq \theta < 90^\circ, 0^\circ \leq \phi \leq 22.08^\circ\}$, which corresponds to the numerical aperture of the objective lens $\text{NA} = 0.5$. The integral response is used to evaluate scattered intensity captured by the objective lens [10].

We use an exciting plane wave with a free space wavelength of $\lambda = 658 \text{ nm}$ and a glass prism having a refractive index of $n_0 = 1.46$. We assume that a PSL particle with a refractive index $n_i = 1.59$ is located in water characterized by a refractive index $n_3 = 1.33$. The glass prism is coated by films of Ti of thickness $d_1 = 3 \text{ nm}$ and refractive index $n_1 = 2.24 - 3.01i$ and Au of thickness $d_2 - d_1 = 10 \text{ nm}$ and $n_2 = 0.164 - 3.22i$. So, an evanescent wave appears at incident angles $\beta_0 > \beta_c$. The critical angle corresponding to $\arcsin(n_3/n_0)$, in this particular case, is $\beta_c \approx 61.05^\circ$. We will mostly use an incident angle $\beta_0 = 63^\circ$. Recall that $\beta_0 = 0^\circ$ corresponds to a plane wave propagating normally to the prism surface.

We start with comparison of computational results for different particle diameters. Figures 2 and 3 demonstrate the objective response (14) versus particle height (h) for different particle diameters between 1 and $0.1 \mu\text{m}$ in the presence of films. For comparison one curve calculated for the plain substrate (without film) is included in each figure. Without layers the decay is almost exponential as expected from previous studies [10]. Smaller deviations from a simple exponential decay increase with decreasing particle diameter.

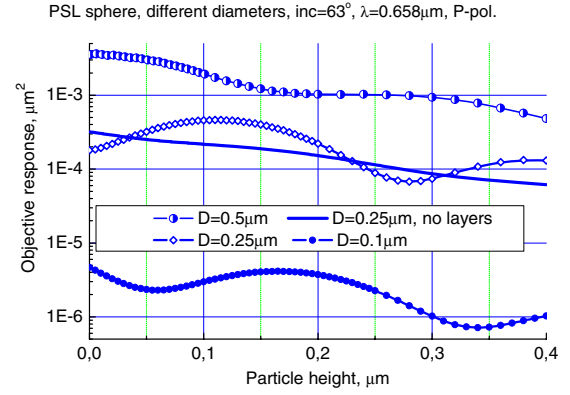


Figure 3. Objective response versus particle height for different particle diameters in the presence of layers and without; P polarization.

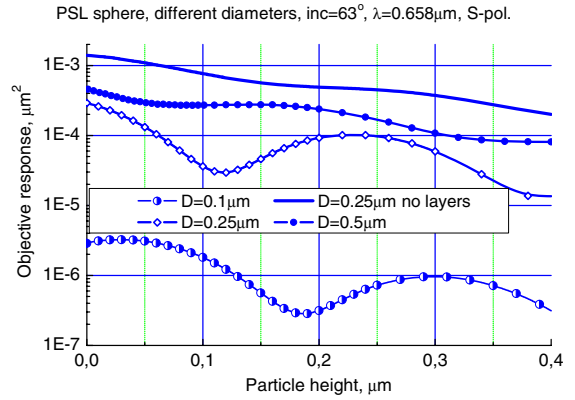


Figure 4. Objective response versus particle height for different particle diameters in the presence of layers and without; S polarization.

In the presence of a Ti/Au bilayer oscillatory deviations from an exponential decay become significant. The amplitude of oscillations also increases with decreasing particle size. In contrast to results for substrates without layers the phase of the superimposed oscillations in figures 2 and 3 strongly depends on the size of the particle. In view of possible TIRM scattering experiments on substrates with strongly reflecting layers, it is noteworthy that for most particle diameters simulated, the intensity distance relation is no longer monotonic. This results in an unambiguous relation between particle-wall distance and scattering intensity. Under these conditions the interpretation of TIRM scattering data will become very challenging if not impossible.

Figure 4 shows a selection of curves calculated for S polarized illumination and otherwise identical parameters as in figures 2 and 3. Qualitatively the features are similar but the oscillations have larger amplitude for S polarized illumination. This can also be seen in the direct comparison between results for S and P polarized illumination and an $0.7 \mu\text{m}$ diameter particle in figure 5. Here a 180° phase shift between the superimposed oscillations for S and P polarized illumination becomes obvious. The fixed phase shift of 180° seems to be independent of the particle diameter, but was not observed for substrates without layers [10].

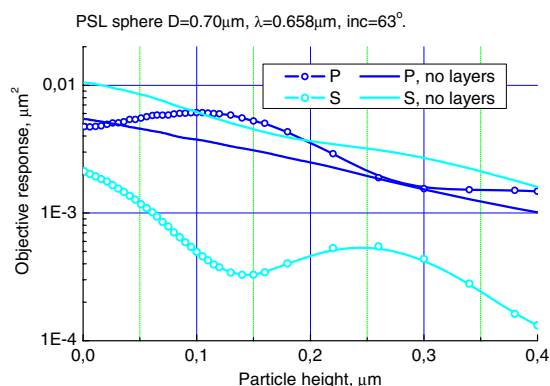


Figure 5. Objective response versus particle height for a particle of diameter $D = 0.7 \mu\text{m}$ in the presence of layers and without; P and S polarizations.

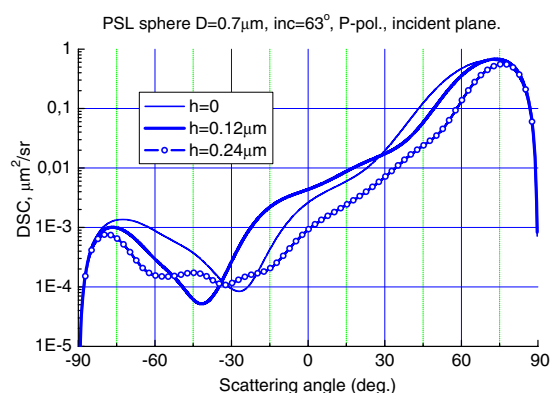


Figure 7. DSC versus scattering angle for a particle of diameter $D = 0.7 \mu\text{m}$ for different heights in the presence of layers; P polarization.

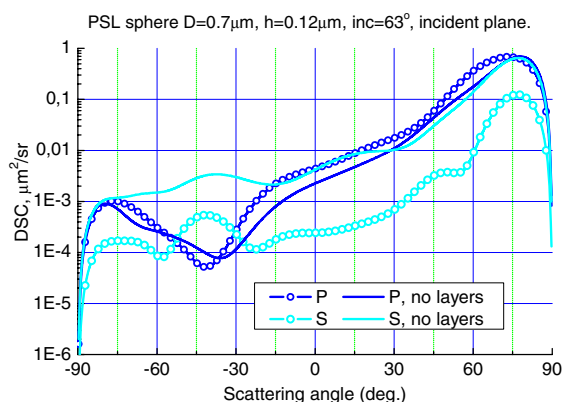


Figure 6. DSC (13) versus scattering angle for a particle of diameter $D = 0.7 \mu\text{m}$, height $h = 0.12 \mu\text{m}$, in the presence of layers and without; P and S polarizations.

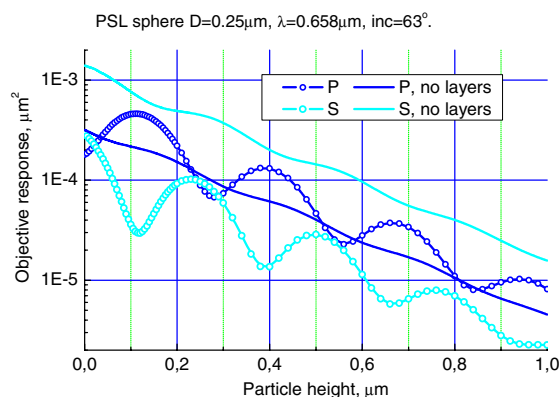


Figure 8. Objective response versus particle height for a particle of diameter $D = 0.25 \mu\text{m}$ in the presence of layers and without; P and S polarizations.

To further investigate the scattering process figure 6 shows results for DSC (13) versus scattering angle in the plane of incidence for a particle of diameter $D = 0.7 \mu\text{m}$ in the presence of layers and without for both polarizations. In general the behaviour of the curves appears similar (decay towards negative scattering angles, pronounced minimum or maximum around -40°); however in the case of layers the DSC has more salient features. This is also the case comparing results for P and S illumination and might account for the stronger oscillations in these cases (compare figures 2–5).

In figure 7 DSC results for the same particle as in figure 6 but different heights above the layers are shown for P polarized excitation, illustrating how the scattering characteristic is significantly altered for different particle–wall distances.

In figures 8–10 similar investigations for a PSL particle of diameter $D = 0.25 \mu\text{m}$ are presented. By comparison with results for a particle of larger diameter $D = 0.7 \mu\text{m}$ as presented in figures 5–7, the oscillating behaviour of the curves in the presence of layers becomes even more obvious if we take wider range of heights (figure 8). Scattering interaction between particle and plane surfaces influences the shape of the scattering patterns.

In figure 11 the dependence of the objective response from the Au layer thickness is presented. One can observe that in

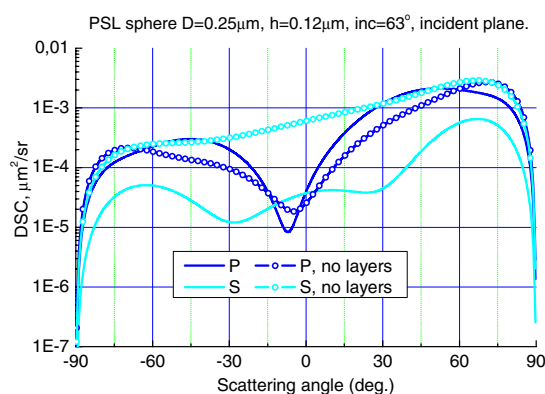


Figure 9. DSC versus scattering angle for a particle of diameter $D = 0.25 \mu\text{m}$, height $h = 0.12 \mu\text{m}$ in the presence of layers and without; P and S polarizations.

spite of the slight decrease of the response with increasing layer thickness, the character of the curves stays the same.

Here we would like to mention that if we omit the absorption of the layers, the amplitude of oscillations becomes much lower. Hence, this effect can be caused by absorption. Another reason for such behaviour could be the particle

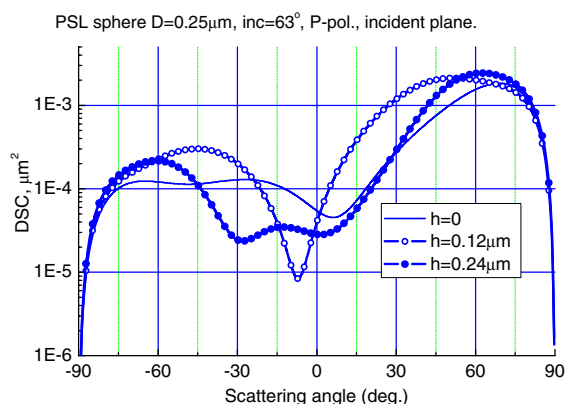


Figure 10. DSC versus scattering angle for a particle of diameter $D = 0.25 \mu\text{m}$ for different heights in the presence of layers; P polarization.

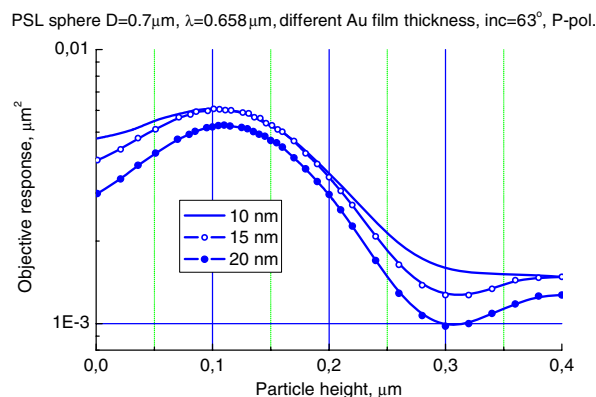


Figure 11. Objective response versus particle height for a particle of diameter $D = 0.7 \mu\text{m}$ for different thicknesses of Au film; P polarization.

interaction with its image with respect to the upper layer. We will investigate this effect in our future research.

From the results presented one can see that layers cause essential changes in scattering properties of the particles. In particular they provide field enhancement in the vicinity of the surface. The presence of layers causes oscillations due to multiple interactions between particles and layered surfaces. With the presence of layers the intensity of P polarization mostly exceeds the intensity of S polarization in contrast to the case for a bare surface.

4. Conclusion

Based on the discrete sources method, a computer model for the analysis of evanescent wave scattering by a spherical particle located near a multilayered glass prism

has been developed. Scattering behaviour of particles and its dependence on height and layer presence have been investigated to demonstrate the capability of the method. From the calculation results one can see that objective response of the particles situated near the multilayered prism surface demonstrates pronounced oscillating character. This effect can be caused by different factors, such as interaction of a particle with its image or layer absorption. We hope that further investigations may help to understand this effect better and to work out recommendations for optimal design of TIRM experiments.

Acknowledgments

The authors would like to thank C Hertlein for helpful discussions. We gratefully acknowledge funding of this research by Deutsche Forschungsgemeinschaft (DFG) and the Russian Foundation for Basic Research (RFBR).

References

- [1] Prieve D C, Luo F and Lanni F 1987 Brownian motion of a hydrosol particle in a colloidal force field *Faraday Discuss. Chem. Soc.* **83** 297–307
- [2] Helden L *et al* 2004 Depletion potentials induced by charged colloidal rods *Langmuir* **20** 5662
- [3] Israelachvili J N 1991 *Intermolecular and Surface Forces* 2nd edn (London: Academic)
- [4] Pashley R M 1995 Atomic force microscopy: a new method for the study of colloidal forces *Sci. Prog.* **78** 173
- [5] Walz J Y 1997 Measuring particle interactions with total internal reflection microscopy *Curr. Opin. Colloid Interface Sci.* **2** 600–6
- [6] Prieve D C 1999 Measurement of colloidal forces with TIRM *Adv. Colloid Interface Sci.* **82** 93–125
- [7] Bike S G 2000 Measuring colloidal forces using evanescent wave scattering *Curr. Opin. Colloid Interface Sci.* **5** 144
- [8] Eremin Y, Orlov N and Sveshnikov A 1999 *Generalized Multipole Techniques for Electromagnetic and Light Scattering* ed T Wriedt (Amsterdam: Elsevier) p 39
- [9] Eremin Y 2000 The method of discrete sources in electromagnetic scattering by axially symmetric structures *J. Commun. Technol. Electron.* **45** 269–80
- [10] Helden L, Eremina E, Eremin Y, Riefler N, Hertlein C, Bechinger C and Wriedt T 2006 Single particle evanescent light scattering simulations for total internal reflection microscopy *Appl. Opt.* **45** 7299–308
- [11] Xia Y and Whitesides G M 1998 Soft lithography *Angew. Chem. Int. Edn* **37** 550–75
- [12] Courjon D 2001 *Near-Field Microscopy and Near-Field Optics* (London: Imperial College Press)
- [13] Eremin Y and Wriedt T 2004 Discrete sources method model for evanescent waves scattering analysis *J. Quant. Spectrosc. Radiat. Transfer* **89** 53–65
- [14] Doicu A, Eremin Yu A and Wriedt T 2001 Scattering of evanescent waves by a particle on or near a plane surface *Comput. Phys. Commun.* **134** 1–10
- [15] Chu W C 1995 *Waves and Fields in Inhomogeneous Media* (New York: IEEE Press)